Observing the Suppression of Superconductivity in $RbEuFe_4As_4$ by Correlated Magnetic Fluctuations

D. Collomb[1],[*] S. J. Bending[1] A. E. Koshelev[2] M. P. Smylie[2,3] L. Farrar[1]
J.-K. Bao[2,4] D. Y. Chung[2] M. G. Kanatzidis[2,5] W.-K. Kwok[2] and U. Welp[2]

[1]*University of Bath, Claverton Down, Bath BA2 7AY, United Kingdom*
[2]*Argonne National Laboratory, Materials Science Division, 9700 South Cass Avenue, Lemont, Illinois 60439, USA*
[3]*Department of Physics and Astronomy, Hofstra University, Hempstead, New York 11549, USA*
[4]*Laboratory of Crystallography, University of Bayreuth, D-95447 Bayreuth, Germany*
[5]*Department of Chemistry, Northwestern University, Evanston, Illinois 60208, USA*

In this Letter, we describe quantitative magnetic imaging of superconducting vortices in $RbEuFe_4As_4$ in order to investigate the unique interplay between the magnetic and superconducting sublattices. Our scanning Hall microscopy data reveal a pronounced suppression of the superfluid density near the magnetic ordering temperature in good qualitative agreement with a recently developed model describing the suppression of superconductivity by correlated magnetic fluctuations. These results indicate a pronounced exchange interaction between the superconducting and magnetic subsystems in $RbEuFe_4As_4$, with important implications for future investigations of physical phenomena arising from the interplay between them.

The interplay between magnetism and superconductivity has intrigued scientists for decades [1–3]. Unlike the coexistence of ferromagnetism and superconductivity in unconventional spin-triplet uranium compounds [4,5], their coexistence in spin-singlet superconductors is generally unfavorable because the magnetic exchange field destroys opposite spin Cooper pairs [1–3]. Nevertheless, a growing number of rare spin-singlet superconductors with a magnetic transition temperature T_m *below* the superconducting transition temperature T_c has been discovered. This includes the rare-Earth (R)-based materials RRh_4B_4 [6], RMo_8S_8 [7], in which magnetic ordering eventually destroys superconductivity, and also the nickel borocarbides with full coexistence of superconductivity and magnetism [8,9]. The magnetic moments in these compounds reside in sublattices that are spatially separated from the superconducting electrons, thus the magnetic exchange interaction is weak enough to allow for the coexistence of superconductivity and magnetism below their respective transition temperatures [10].

One family with growing prominence in this field is the europium-containing iron pnictides [11,12]. These typically exhibit high T_c's in excess of 30 K and somewhat lower magnetic ordering temperatures (15–20 K). Hence, the strong superconducting pairing, relatively large magnetic exchange interaction, and wide temperature window makes them ideal materials to investigate emerging new physical phenomena. Unlike the Eu-122 compounds, which require doping [13–17], or the application of pressure to obtain superconducting and magnetic

transitions [18,19], the stoichiometric 1144 compounds (e.g., $RbEuFe_4As_4$ and $CsEuFe_4As_4$) yield both under ambient conditions [20–23]. The Eu atoms in $RbEuFe_4As_4$ carry large, spin-only moments that undergo long-range ordering at 15 K. Below the magnetic transition temperature, these moments exhibit in-plane alignment, and there is a large anisotropy of the in-plane and out-of-plane exchange constants [24]. This makes it distinct from materials where the moments order along the c axis, which can create their own unique states of vortex matter linked to ferromagnetic stripe domain structures, such as in $EuFe_2(As_{0.79}P_{0.21})_2$ [25]. Neutron scattering experiments on $RbEuFe_4As_4$ have revealed helical ordering of successive layers with a period of four unit cells along the c axis due to a weak antiferromagnetic exchange interaction in this direction [26].

Although the magnetic structure in $RbEuFe_4As_4$ is now quite well understood, its impact on the coexisting superconductivity is still unclear. Above the magnetic ordering temperature fluctuating magnetic moments are thought to suppress superconductivity via magnetic scattering [27–29], while in the vicinity of T_m these moments become strongly correlated, further enhancing this suppression [30–32]. Optical conductivity measurements probing the $RbEuFe_4As_4$ superconducting gap revealed a small drop in $\Delta(T)$ as T_m is approached from above, followed by a recovery at lower temperatures [33]. Additionally, magnetic force microscopy (MFM) imaging of vortices revealed a gradual reduction in vortex density below $\sim$18 K, which drops to a weak minimum at $\sim$12 K and

recovers again at lower temperatures, further hinting at a weak interaction between the superconducting and magnetic subsystems [33]. The analysis of the MFM measurements was, however, limited to counting vortex numbers as a function of temperature, rather than a direct investigation of the vortex structures themselves. On the other hand, recent angle-resolved photoemission spectroscopy (ARPES) reveals no significant suppression of the superconducting gaps around the magnetic ordering temperature and density-functional theory calculations show that the topology and orbital character of the Fe3d bands do not strongly depend on the magnetic order, although the band structure evidently exhibits a degree of sensitivity to it [34]. However, these measurements would not capture the full impact of the effect of magnetic fluctuations on superconductivity, as the relative exchange correction to the gap is predicted to be significantly smaller than the correction to the superfluid density [32]. Here we use high-resolution scanning Hall microscopy (SHM) to investigate the influence of magnetism on individual superconducting vortices and directly extract the temperature dependence of the penetration depth $\lambda(T)$ and the superfluid density $\rho_s(T)$. This approach has the advantage that it is not influenced by the statistical nature of vortex patterns or by internal flux pumping effects by the magnetic sublattice [35].

The exchange interaction between the localized moments and Cooper pairs is expected to suppress the superfluid density. In the paramagnetic phase, in the regime when the exchange-field correlation length ξ_h is much smaller than the in-plane coherence length ξ_s, this suppression is caused by magnetic scattering and very similar to the case of magnetic impurities [28,29]. However, as the correlation length diverges for $T \rightarrow T_m$, it always exceeds ξ_s in the vicinity of T_m leading to a different "smooth" regime of interaction between the magnetic and superconducting subsystems. In the case of RbEuFe$_4$As$_4$, ξ_s is very small [24,36], resulting in a smooth regime across a significant temperature range. The crossover between these "scattering" and smooth regimes has been quantitatively described in Ref. [32] and results are summarized in the Supplemental Material [37]. The correction to ρ_s has two main temperature dependencies: via the ratio $T/\Delta_0(T)$, and via the correlation length $\xi_h(T)$. In the vicinity of T_m, the second of these dependencies is expected to dominate, whereas across a wider temperature range both are expected to contribute.

We have used SHM to image discrete vortices in high-quality RbEuFe$_4$As$_4$ crystals and studied the influence of the emerging magnetic order on the penetration depth $\lambda(T)$ and the superfluid density $\rho_s(T)$ [38]. SHM has the advantage of being a quantitative and noninvasive magnetic imaging technique that allows the magnetic penetration depth to be directly obtained from model fits. The temperature-dependent superfluid density has then been calculated assuming $\rho_s(T) \propto \lambda(T)^{-2}$ and exhibits a very substantial

drop in the vicinity of T_m. A direct comparison between our data and the model suggests that there must be a noticeable exchange interaction between the Eu^{2+} moments and Cooper pairs that substantially suppresses superconductivity near T_m. A recovery of the superfluid density at lower temperatures reflects a reduction of the magnetic correlation length and resulting weakening of the magnetic scattering. The good qualitative agreement with our model represents an important step forward in our understanding of the subtle physics at play in magnetic superconductors.

High-quality single crystals of RbEuFe$_4$As$_4$ were grown using a RbAs flux, yielding flat, rectangular plateletlike crystals with lateral dimensions up to $\sim$1 mm in the ab plane and thickness $\sim$60 μm parallel to the c axis [22]. X-ray diffraction and specific heat measurements have previously confirmed that the crystals are single-phase material without EuFe$_2$As$_2$ inclusions [22]. RbEuFe$_4$As$_4$ has a simple tetragonal structure and a $P4/mmm$ space group, with one formula per unit cell and lattice constants $a = b = 3.88$ and $c = 13.27$ Å [22]. A single unit cell of the crystal structure and atom-to-atom bonding is shown in the inset of Fig. 1. The high quality of the crystals was confirmed via electronic transport and magnetization data. The transport measurements were performed by attaching gold wires with silver paint in a standard four-lead Hall bar configuration, and the in-plane resistivity then measured as a function of temperature. This is shown in Fig. 1, revealing a superconducting transition of $\sim$37 K. The magnetic susceptibility as a function of temperature was measured with a commercial magnetic property measurement system (MPMS3, Quantum Design) with magnetic fields applied along the c axis revealing a magnetic transition at $\sim$15 K.
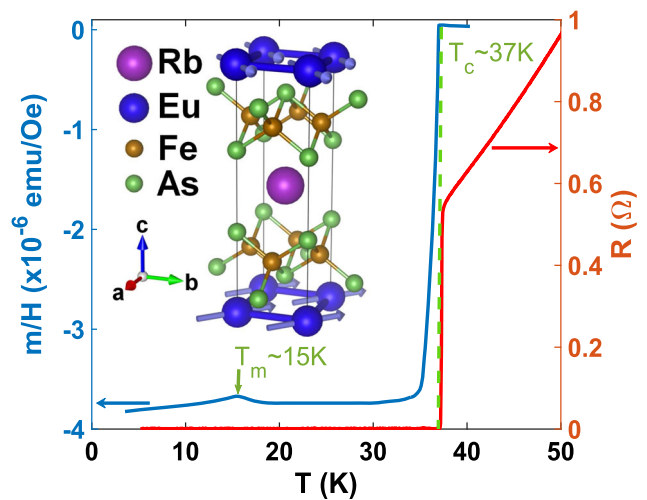

FIG. 1. Temperature dependence of the in-plane resistivity of RbEuFe$_4$As$_4$ near the superconducting transition and the magnetic susceptibility of a zero-field-cooled RbEuFe$_4$As$_4$ single crystal with a 10 Oe magnetic field applied along the c axis. The inset shows one unit cell of RbEuFe$_4$As$_4$, where the magnetic structure of the Eu sublattice is indicated.
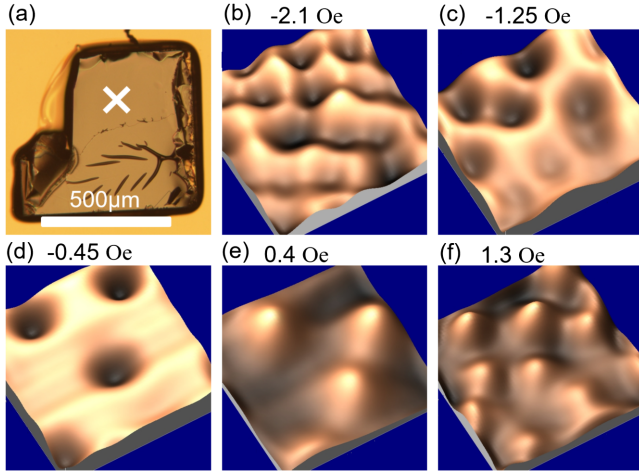
FIG. 2. (a) Optical micrograph of a $RbEuFe_4As_4$ single crystal after cleaving and deposition of a conductive coating. The approximate location of the images taken in Fig. 3 is marked by the white cross. (b)–(f) Three-dimensional SHM images of vortices in a $RbEuFe_4As_4$ single crystal after field cooling to 30 K in effective perpendicular fields between -2.1 and 1.3 Oe [39]. The scan size is 12.6×12.6 μm. The full magnetic field range of the images (vertical scale) span 0.4 (-2.1), 0.5 (-1.25), 0.8 (-0.45), 0.7 (0.4), 0.5 G (1.3 Oe).

To prepare samples for SHM, a crystal of $RbEuFe_4As_4$ was glued flat on a gold-coated Si substrate and mechanically cleaved immediately prior to coating with a Cr(5 nm)/Au(40 nm) film [cf. Fig. 2(a)]. This ensured good electrical contact between the scanning tunneling microscopy (STM) tunneling tip on the SHM sensor and the sample surface. The Hall probe used was based on a GaAs/AlGaAs heterostructure two-dimensional electron gas defined by the intersection of two 700 nm wide wires. This was located ~ 5 μm from the gold-coated corner of a deep mesa etch acting as the STM tip [38]. The Hall probe was mounted at an angle of approximately 1° with respect to the sample plane, ensuring that the STM tip is always the closest point to the sample surface. The Hall probe was approached to the sample until a threshold tunnel current was reached, at which point the probe was manually lifted out of tunneling by ~ 50 nm for rapid flying mode scanning. From this, a two-dimensional map of the magnetic induction across the surface of the sample was obtained [38], and several images were then averaged frame by frame to suppress low-frequency noise from the Hall probe.

Figures 2(b)–2(f) display vortex-resolved SHM images for a $RbEuFe_4As_4$ crystal after field cooling to 30 K from above T_c at various small, perpendicular effective magnetic fields between -2.1 and 1.3 Oe. Note that quoted values of magnetic field are effective ones after we have accounted for small amounts of flux that get trapped in our superconducting magnet upon initial cool down. This remanent field has been estimated by counting the number of vortices in our field of view at various applied fields [37]. The scan range of the piezoelectric scanner is strongly temperature dependent and varies from $8.5 \times 8,5$ to 13.5×13.5 μm between 10 and 35 K. Even below T_m, we can attribute all the magnetic contrast in the images to vortices and see no sign of c-axis fields associated with domain walls between magnetic domains. This differs from the MFM images in Ref. [33], which showed the presence of such stray magnetic fields at temperatures below T_m. It is possible that these domain-wall fields are also present in our sample on much larger length scales than we probe in our measurements.

A sample was then field cooled at $H_z^{eff} = -0.8$ Oe from the normal state and images captured at several fixed temperatures down to 10 K [cf. Figs. 3(a)–3(c)]. Profiles of one particular vortex at a few selected temperatures are presented in Fig. 3(d). The influence of the long-range magnetic ordering is clearly reflected in the peak amplitude of the vortex, which weakens (and broadens) as we approach 15 K from above. The amplitude then starts to grow again at lower temperatures. The same behavior is observed in our detailed analysis of the temperature dependence of four distinct vortices in two different crystals. We also observe an unexpected increase in low-frequency noise in our images between 20 and 15 K in a regime where the intrinsic Hall sensor noise would normally fall as the temperature is lowered, see Supplemental Material [37] for more details. We tentatively associate this additional noise with magnetic fluctuations near the sample surface that have not been screened out by superconductivity. We also checked that there was no detectable hysteresis in the influence of the long-range magnetic order on the vortices by capturing images at both increasing and decreasing temperatures.

To investigate this behavior further, we have performed a quantitative analysis of the temperature-dependent vortex profiles $B_z(x_0, z, \lambda)$ by fitting them to a modified Clem model [40,41] to extract the magnetic penetration depth $\lambda(T)$,

$$B_z(x_0, z, \lambda) = \frac{\Phi_0}{2\pi w^2 \lambda K_1\left(\frac{\xi_s}{\lambda}\right)} \int_{-w/2}^{w/2} dy \int_{x_0-w/2}^{x_0+w/2} dx \int_0^\infty q dq \frac{K_1(\sqrt{q^2 + \lambda^{-2}}\xi_s) \exp(-qz) J_0(q\sqrt{x^2 + y^2})}{\sqrt{q^2 + \lambda^{-2}} + q}, \qquad (1)$$

where z is the sensor scan height measured from the sample surface, $w = 0.5$ μm is the electronic width of the Hall probe, q is the Fourier wave vector, K_1 and J_0 are Bessel functions, ξ_s is the coherence length for which we assume $\xi_s = 1.46$ nm$/\sqrt{1 - T/T_c}$, and Φ_0 is the flux quantum. Fits to Eq. (1) have been superimposed on the measured
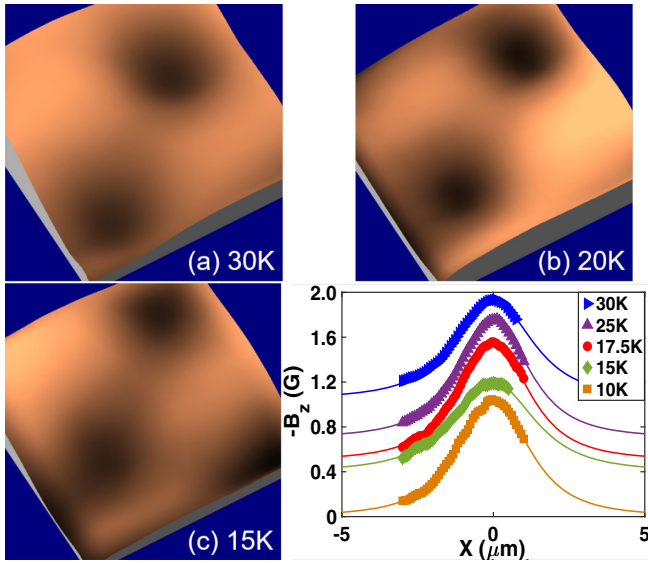
FIG. 3. (a)–(c) Vortex-resolved SHM images after field cooling in $H_z^{\text{eff}} = -0.8$ Oe from above T_c to three different temperatures, illustrating the evolution of vortex profiles as T_m is approached from above. The field of view in each of these images is 6.5×6.5 μm and vertical scales span 0.9 G. (d) Vortex profiles extracted from SHM images in the sequence shown in (a)–(c) with superimposed fits to a modified Clem model, Eq. (1).
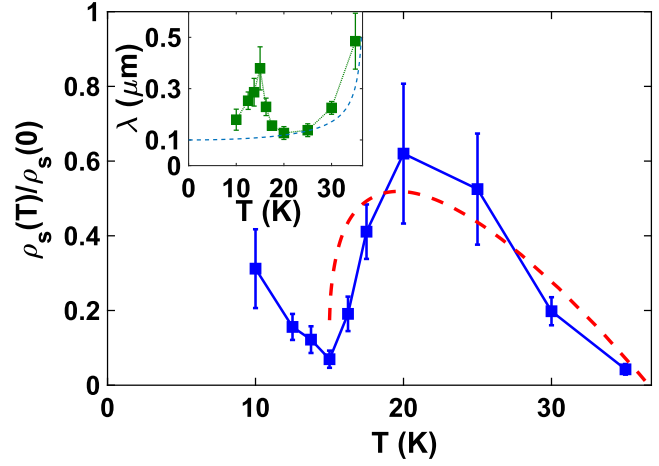

FIG. 4. Temperature dependence of the normalized superfluid density $\rho_s(T)/\rho_s(0)$ (solid symbols) and a fit to the model described in the text (dashed line). Inset: plot of the penetration depth as a function of temperature extracted from fits to a modified Clem model, Eq. (1), for one of the vortices shown in Figs. 3(a)–3(c). The dashed light blue line shows the assumed bare penetration depth dependence $\lambda_0(T) = \lambda(0)/\sqrt{1 - (T/T_c)^2}$.

profiles in Fig. 3(d) showing excellent agreement. The value of $z = 1.45 \pm 0.01$ μm was extracted from a fit at 30 K with $\lambda(30\text{ K})$ estimated from experimental data using Ginzburg-Landau theory expressions for the specific heat jump and upper critical field slope at T_c (cf. Supplemental Material [37]). This is consistent with the sensor tilt angle used. The same scan height was maintained at all other temperatures and, although it is large compared to the penetration depth we are trying to measure, we are nevertheless able to extract values of $\lambda(T)$ from fits with good accuracy. The temperature dependence of the extracted London penetration depth $\lambda(T)$ is shown in the inset of Fig. 4, while the corresponding normalized superfluid density $\rho_s(T)/\rho_s(0) = \lambda(0)^2/\lambda(T)^2$ is plotted in the main panel of this figure. The vertical error bars on experimental data points reflect the impact of the sensor noise level on the vortex profile fitting process combined with uncertainties in the estimated scan height z.

The most natural mechanism of the observed significant enhancement of the vortex diameter near T_m is suppression of superconductivity due to exchange interaction between Cooper pairs and localized Eu^{2+} moments. This enhancement becomes especially pronounced in the vicinity of the magnetic transition, where the moments become strongly correlated. The quantitative description of the suppression of superconducting parameters by correlated magnetic fluctuations has been elaborated in Ref. [32]. In the Supplemental Material [37], we summarize the results for the correction to the superfluid density that we use

for the modeling of the data. The relative correction is proportional to the square of the amplitude of the exchange field h_0 and depends on two ratios, $T/\Delta_0(T)$ and $\xi_s(T)/\xi_h(T)$. We also account for renormalization of parameters due to the nonlocality of the exchange interaction described by the range a_J, $\xi_h^2 = \xi_S^2 + 2a_J^2$ and $\tilde{h}_0^2 = h_0^2\xi_S^2/\xi_h^2$, where ξ_S is the spin correlation length. We assume the Berezinskii-Kosterlitz-Thouless (BKT) shape for the latter, $\xi_S(T) = a\exp[b\sqrt{T_m/(T - T_m)}]$, based on recent experimental observations [42], where $a = 0.39$ nm is the in-plane Eu atom spacing, and we use the numerical factor b as a fit parameter.

We plot the results of our model as a dashed line alongside our data using the amplitude of the exchange field, $h_0 = 15$ K, a zero temperature superconducting gap $\Delta(0) = 2$ meV, a BKT constant $b = 1$, and the nonlocality range $a_J = 3a$. We use the BCS temperature dependence to describe $\Delta(T)$, which is corrected in the model for the magnetic exchange interaction. The Ginzburg-Landau coherence length is estimated to be $\xi^{\text{GL}} = 1.46$ nm, deduced from the linear slope of the c-axis upper critical field near T_c [24,36]. The exchange correction is added to the bare penetration depth $\lambda_0(T)$ that would be realized in the absence of any exchange interactions with magnetic fluctuations, for which we assume a simple phenomenological temperature dependence $\lambda_0(T) = \lambda(0)/\sqrt{1 - (T/T_c)^2}$. We apply a value of $\lambda(0) = 100$ nm which has been estimated from fitting the aforementioned dependence to our extracted penetration depths from 20 K and above. This value provides a better

description across all temperatures above 20 K than the value $\lambda(0) = 133$ nm extracted from the thermodynamic data using the Ginzburg-Landau theory [37].

The strong suppression of superfluid density in the vicinity of T_m is remarkable and was not previously observed in RbEuFe$_4$As$_4$ or indeed any other ferromagnetic superconductor, although this possibility was recently suggested by Willa *et al.* [36]. This is also in apparent conflict with the analysis of recent ARPES measurements, which concluded that the two sublattices are almost fully decoupled [34]. To understand the temperature-dependent trend of the suppression seen in our data in Fig. 4, we turn to our model. Comparing the measured normalized ρ_s with predictions of the model, we find good qualitative agreement with our 2D BKT description of the magnetic correlations above the magnetic transition temperature $T_m = 15$ K, confirming the nature of the ordering and its impact through $\xi_h(T)$ on superconductivity in the vicinity of T_m. The temperature-dependent magnetic correlation length $\xi_h(T)$, which is governed by the constant b, is responsible for the wide temperature range over which the magnetic ordering influences the superconducting parameters. Above T_m, the suppression decreases rapidly as temperature increases, while the shift in T_c is ∼1 K. Although the suppression of superfluid density is quite large, the fitted magnetic exchange constant remains moderate at $h_0 \approx 0.4T_c$. This is still significantly smaller than exchange constants estimated for the ternary compounds, which are several orders of magnitude larger than T_c [3]. This suggests a weak enough coupling between Eu moments and Cooper pairs in our material that superconductivity is never destroyed, yet one that is strong enough to have a substantial impact on the superconducting parameters near T_m. We emphasize that our model is a qualitative one and at best only qualitative agreement with our data is expected. In particular, the model assumes two-dimensional scattering behavior across the whole temperature range $T > T_m$, while this assumption must break down in the vicinity of the magnetic transition where a crossover to a three-dimensional regime takes place. In addition, the BCS expressions we have used for the temperature dependence of the gap and penetration depth were derived for single-band materials, whereas RbEuFe$_4$As$_4$ has a more complicated multiband structure. Nevertheless, the qualitative agreement between the model and data validates our simple assumptions in this fascinating magnetic superconducting material.

In conclusion, we have directly quantified the temperature-dependent superfluid density in RbEuFe$_4$As$_4$ crystals to reveal a significant suppression of superconductivity due to correlated quasi-two-dimensional magnetic fluctuations, despite the apparent spatial separation of the two sublattices. Although insufficient to completely destroy superconductivity, this suggests a significant influence of the exchange interaction on the superconducting subsystem.

Our results will stimulate additional investigations into the properties of RbEuFe$_4$As$_4$ and other magnetic superconductors, building on the existing analytical model.

*d.collomb@bath.ac.uk

[1] P. Fulde and J. Keller, Theory of magnetic superconductors, in *Superconductivity in Ternary Compounds II*, edited by M. B. Maple and Ø. Fischer (Springer, New York, 1982), pp. 249–294.

[2] L. Bulaevskii, A. Buzdin, M. Kulić, and S. Panjukov, Coexistence of superconductivity and magnetism theoretical predictions and experimental results, Adv. Phys. **34**, 175 (1985).

[3] M. L. Kulić and A. I. Buzdin, Coexistence of singlet superconductivity and magnetic order in bulk magnetic superconductors and sf heterostructures, in *Superconductivity: Conventional and Unconventional Superconductors*, edited by K. H. Bennemann and J. B. Ketterson (Springer, Berlin, Heidelberg, 2008), p. 163.

[4] S. Saxena, P. Agarwal, K. Ahilan, F. Grosche, R. Haselwimmer, M. Steiner, E. Pugh, I. Walker, S. Julian, P. Monthoux *et al.*, Superconductivity on the border of itinerant-electron ferromagnetism in UGe$_2$, Nature (London) **406**, 587 (2000).

[5] D. Aoki, K. Ishida, and J. Flouquet, Review of *u*-based ferromagnetic superconductors: Comparison between UGe$_2$, URhGe, and UCoGe, J. Phys. Soc. Jpn. **88**, 022001 (2019).

[6] M. B. Maple, H. C. Hamaker, and L. D. Woolf, Superconductivity, magnetism and their mutual interaction in ternary rare earth rhodium borides and some ternary rare Earth transition metal stannides, in *Superconductivity in Ternary Compounds II*, edited by M. B. Maple and Ø. Fischer (Springer, New York, 1982), pp. 99–141.

[7] M. B. Maple and Ø. Fischer, Magnetic superconductors, in *Superconductivity in Ternary Compounds II*, edited by M. B. Maple and Ø. Fischer (Springer, New York, 1982), pp. 1–10.

[8] K. H. Müller and V. N. Narozhnyi, Interaction of superconductivity and magnetism in borocarbide superconductors, Rep. Prog. Phys. **64**, 943 (2001).

[9] D. Wulferding, I. Yang, J. Yang, M. Lee, H. C. Choi, S. L. Bud'ko, P. C. Canfield, H. W. Yeom, and J. Kim, Spatially

resolved penetration depth measurements and vortex manipulation in the ferromagnetic superconductor ErNi$_2$B$_2$C, Phys. Rev. B **92**, 014517 (2015).

[10] H. Eisaki, H. Takagi, R. J. Cava, B. Batlogg, J. J. Krajewski, W. F. Peck, K. Mizuhashi, J. O. Lee, and S. Uchida, Competition between magnetism and superconductivity in rare-Earth nickel boride carbides, Phys. Rev. B **50**, 647 (1994).

[11] G.-H. Cao, W.-H. Jiao, Y.-K. Luo, Z. Ren, S. Jiang, and Z.-A. Xu, Coexistence of superconductivity and ferromagnetism in iron pnictides, J. Phys. Conf. Ser. **391**, 012123 (2012).

[12] S. Zapf and M. Dressel, Europium-based iron pnictides: A unique laboratory for magnetism, superconductivity and structural effects, Rep. Prog. Phys. **80**, 016501 (2017).

[13] Z. Ren, Q. Tao, S. Jiang, C. Feng, C. Wang, J. Dai, G. Cao, and Z. Xu, Superconductivity Induced by Phosphorus Doping and Its Coexistence with Ferromagnetism in EuFe$_2$(As$_{0.7}$P$_{0.3}$)$_2$, Phys. Rev. Lett. **102**, 137002 (2009).

[14] H. S. Jeevan, Z. Hossain, D. Kasinathan, H. Rosner, C. Geibel, and P. Gegenwart, High-temperature superconductivity in Eu$_{0.5}$K$_{0.5}$Fe$_2$As$_2$, Phys. Rev. B **78**, 092406 (2008).

[15] J. Maiwald, H. S. Jeevan, and P. Gegenwart, Signatures of quantum criticality in hole-doped and chemically pressurized EuFe$_2$As$_2$ single crystals, Phys. Rev. B **85**, 024511 (2012).

[16] Anupam, P. L. Paulose, S. Ramakrishnan, and Z. Hossain, Doping dependent evolution of magnetism and superconductivity in Eu$_{1-x}$K$_x$Fe$_2$As$_2$($x = 0$–1) and temperature dependence of the lower critical field H$_{c1}$, J. Phys. Condens. Matter **23**, 455702 (2011).

[17] Y. Qi, L. Wang, Z. Gao, X. Zhang, D. Wang, C. Yao, C. Wang, C. Wang, and Y. Ma, Superconductivity at 34.7 K in the iron arsenide Eu$_{0.7}$Na$_{0.3}$Fe$_2$As$_2$, New J. Phys. **14**, 033011 (2012).

[18] C. F. Miclea, M. Nicklas, H. S. Jeevan, D. Kasinathan, Z. Hossain, H. Rosner, P. Gegenwart, C. Geibel, and F. Steglich, Evidence for a reentrant superconducting state in EuFe$_2$As$_2$ under pressure, Phys. Rev. B **79**, 212509 (2009).

[19] K. Matsubayashi, K. Munakata, M. Isobe, N. Katayama, K. Ohgushi, Y. Ueda, Y. Uwatoko, N. Kawamura, M. Mizumaki, N. Ishimatsu, M. Hedo, and I. Umehara, Pressure-induced changes in the magnetic and valence state of EuFe$_2$As$_2$, Phys. Rev. B **84**, 024502 (2011).

[20] Y. Liu, Y.-B. Liu, Z.-T. Tang, H. Jiang, Z.-C. Wang, A. Ablimit, W.-H. Jiao, Q. Tao, C.-M. Feng, Z.-A. Xu, and G.-H. Cao, Superconductivity and ferromagnetism in hole-doped RbEuFe$_4$As$_4$, Phys. Rev. B **93**, 214503 (2016).

[21] K. Kawashima, T. Kinjo, T. Nishio, S. Ishida, H. Fujihisa, Y. Gotoh, K. Kihou, H. Eisaki, Y. Yoshida, and A. Iyo, Superconductivity in Fe-based compound Eu*A*Fe$_4$As$_4$ (*A* = Rb and Cs), J. Phys. Soc. Jpn. **85**, 064710 (2016).

[22] J.-K. Bao, K. Willa, M. P. Smylie, H. Chen, U. Welp, D. Y. Chung, and M. G. Kanatzidis, Single crystal growth and study of the ferromagnetic superconductor RbEuFe$_4$As$_4$, Crystal Growth Des. **18**, 3517 (2018).

[23] Y. Liu, Y.-B. Liu, Q. Chen, Z.-T. Tang, W.-H. Jiao, Q. Tao, Z.-A. Xu, and G.-H. Cao, A new ferromagnetic superconductor: CsEuFe$_4$As$_4$, Sci. Bull. **61**, 1213 (2016).

[24] M. P. Smylie, K. Willa, J.-K. Bao, K. Ryan, Z. Islam, H. Claus, Y. Simsek, Z. Diao, A. Rydh, A. E. Koshelev, W.-K. Kwok, D. Y. Chung, M. G. Kanatzidis, and U. Welp, Anisotropic superconductivity and magnetism in single-crystal RbEuFe$_4$As$_4$, Phys. Rev. B **98**, 104503 (2018).

[25] V. S. Stolyarov, I. S. Veshchunov, S. Y. Grebenchuk, D. S. Baranov, I. A. Golovchanskiy, A. G. Shishkin, N. Zhou, Z. Shi, X. Xu, S. Pyon, Y. Sun, W. Jiao, G.-H. Cao, L. Y. Vinnikov, A. A. Golubov, T. Tamegai, A. I. Buzdin, and D. Roditchev, Domain Meissner state and spontaneous vortex-antivortex generation in the ferromagnetic superconductor EuFe$_2$(As$_{0.79}$P$_{0.21}$)$_2$, Sci. Adv. **4**, 1061 (2018).

[26] K. Iida, Y. Nagai, S. Ishida, M. Ishikado, N. Murai, A. D. Christianson, H. Yoshida, Y. Inamura, H. Nakamura, A. Nakao, K. Munakata, D. Kagerbauer, M. Eisterer, K. Kawashima, Y. Yoshida, H. Eisaki, and A. Iyo, Coexisting spin resonance and long-range magnetic order of Eu in EuRbFe$_4$As$_4$, Phys. Rev. B **100**, 014506 (2019).

[27] A. A. Abrikosov and L. P. Gor'kov, Contribution to the theory of superconducting alloys with paramagnetic impurities, Zh. Eksp. Teor. Fiz. **39**, 1781 (1960) [Sov. Phys. JETP **12**, 1243 (1961)].

[28] S. Skalski, O. Betbeder-Matibet, and P. R. Weiss, Properties of superconducting alloys containing paramagnetic impurities, Phys. Rev. **136**, A1500 (1964).

[29] V. G. Kogan, R. Prozorov, and V. Mishra, London penetration depth and pair breaking, Phys. Rev. B **88**, 224508 (2013).

[30] D. Rainer, Influence of correlated spins on the superconducting transition temperature, Z. Phys. **252**, 174 (1972).

[31] K. Machida and D. Youngner, Superconductivity of ternary rare-Earth compounds, J. Low Temp. Phys. **35**, 449 (1979).

[32] A. E. Koshelev, Suppression of superconducting parameters by correlated quasi-two-dimensional magnetic fluctuations, Phys. Rev. B **102**, 054505 (2020).

[33] V. S. Stolyarov, A. Casano, M. A. Belyanchikov, A. S. Astrakhantseva, S. Y. Grebenchuk, D. S. Baranov, I. A. Golovchanskiy, I. Voloshenko, E. S. Zhukova, B. P. Gorshunov, A. V. Muratov, V. V. Dremov, L. Y. Vinnikov, D. Roditchev, Y. Liu, G.-H. Cao, M. Dressel, and E. Uykur, Unique interplay between superconducting and ferromagnetic orders in EuRbFe$_4$As$_4$, Phys. Rev. B **98**, 140506(R) (2018).

[34] T. K. Kim, K. Pervakov, D. Evtushinsky, S. W. Jung, G. Poelchen, K. Kummer, V. A. Vlasenko, V. M. Pudalov, D. Roditchev, V. S. Stolyarov, D. Vyalikh, V. Borisov, R. Valent1, A.Ernst, S. Eremeev, and E. V. Chulkov, When superconductivity does not fear magnetism: Insight into electronic structure of EuRbFe$_4$As$_4$, arXiv:2008.00736.

[35] V. K. Vlasko-Vlasov, A. E. Koshelev, M. Smylie, J.-K. Bao, D. Y. Chung, M. G. Kanatzidis, U. Welp, and W.-K. Kwok, Self-induced magnetic flux structure in the magnetic superconductor RbEuFe$_4$As$_4$, Phys. Rev. B **99**, 134503 (2019).

[36] K. Willa, R. Willa, J.-K. Bao, A. E. Koshelev, D. Y. Chung, M. G. Kanatzidis, W.-K. Kwok, and U. Welp, Strongly fluctuating moments in the high-temperature magnetic superconductor RbEuFe$_4$As$_4$, Phys. Rev. B **99**, 180502 (R) (2019).

[37] See Supplemental Material at http://link.aps.org/supplemental/10.1103/PhysRevLett.126.157001, which includes a description of the model and the details on how the magnetic noise measurements were performed, including its results.

[38] S. J. Bending, Local magnetic probes of superconductors, Adv. Phys. **48**, 449 (1999).

[39] I. Horcas, R. Fernández, J. Gomez-Rodriguez, J. Colchero, J. Gómez-Herrero, and A. Baro, WSXM: A software for scanning probe microscopy and a tool for nanotechnology, Rev. Sci. Instrum. **78**, 013705 (2007).

[40] J. R. Clem, Simple model for the vortex core in a type ii superconductor, J. Low Temp. Phys. **18**, 427 (1975).

[41] J. R. Kirtley, C. Kallin, C. W. Hicks, E.-A. Kim, Y. Liu, K. A. Moler, Y. Maeno, and K. D. Nelson, Upper limit on spontaneous supercurrents in Sr_2RuO_4, Phys. Rev. B **76**, 014526 (2007).

[42] M. Hemmida, N. Winterhalter-Stocker, D. Ehlers, H.-A. K. von Nidda, M. Yao, J. Bannies, E. Rienks, R. Kurleto, C. Felser, B. Büchner *et al.*, Topological magnetic order and superconductivity in $EuRbFe_4As_4$, arXiv:2010.02110.